LETTER Communicated by Anthony Burkitt

Stochastic Properties of Coincidence-Detector Neural Cells

Ram Krips
ram@eng.tau.ac.il
Miriam Furst
mira@eng.tau.ac.il
Department of Electrical Engineering-Systems, Faculty of Engineering, Tel-Aviv University, Tel-Aviv 69978, Israel

Neural information is characterized by sets of spiking events that travel within the brain through neuron junctions that receive, transmit, and process streams of spikes. Coincidence detection is one of the ways to describe the functionality of a single neural cell. This letter presents an analytical derivation of the output stochastic behavior of a coincidence detector (CD) cell whose stochastic inputs behave as a nonhomogeneous Poisson process (NHPP) with both excitatory and inhibitory inputs. The derivation, which is based on an efficient breakdown of the cell into basic functional elements, results in an output process whose behavior can be approximated as an NHPP as long as the coincidence interval is much smaller than the refractory period of the cell's inputs. Intuitively, the approximation is valid as long as the processing rate is much faster than the incoming information rate. This type of modeling is a simplified but very useful description of neurons since it enables analytical derivations. The statistical properties of single CD cell's output make it possible to integrate and analyze complex neural cells in a feedforward network using the methodology presented here. Accordingly, basic biological characteristics of neural activity are demonstrated, such as a decrease in the spontaneous rate at higher brain levels and improved signal-to-noise ratio for harmonic input signals.

1 Introduction

Neural activity is characterized by sets of spiking events that travel within the brain through neuron junctions that receive, transmit and process stream of spikes (Rieke, Warland, van Steveninck, & Bialek, 1997; Kandel, Schwartz, & Jessell, 2000). These spiking events are stochastic in nature, starting at the peripheral end (Kiang, 1965; Teich & Khanna, 1985; Teich, Heneghan, Lowen, Ozaki, & Kaplan, 1997), and reach higher processing levels (e.g., Abeles, 1982).

The stochastic properties of the auditory neural system have been studied since the 1950s. Spontaneous neural activity was best described as a

homogeneous point Poisson process provided that refractory time was ignored (Rodieck, Kiang, & Gerstein, 1962). Further investigations of the auditory system revealed a description of the neural response as a nonhomogeneous Poisson point process (NHPP) whose instantaneous rate depends on the input stimuli (Rieke et al., 1997; Gray, 1967). These studies ignored the discharge history including the refractory period. Other studies tested the effect of discharge history on depletion in response rate (Gaumond, Kima, & Molnar, 1983) while others modeled the neural response as a doubly stochastic fractal point process (Teich, 1989) or as modified NHPP (Johnson & Swami, 1983; Carney, 1993).

Analysis of the stochastic properties of each level in the brain and of each type of neural cell is essential for characterizing the neural system behavior as a function of input stimuli. In this letter, we concentrate on fundamental coincidence detectors (CD) that receive independent excitatory and inhibitory inputs and generate a spike if the number of excitatory inputs exceeds the number of inhibitory inputs by a known number during a short interval.

In the auditory system, coincidence detectors cells are found in several brainstem nuclei. Such cells are mainly involved in estimating interaural differences, which are the primary acoustical cues for sound localization. They were found in both the superior olivary complex (SOC) and the inferior colliculus (IC) (Rose, Brugge, Anderson, & Hind, 1967; Goldberg & Brown, 1969; Yin & Chan, 1990; McAlpine, Jiang, Shackleton, & Palmer, 1998; Park, 1998; Joris, Smith, & Yin, 1998; Agmon-Snir, Carr, & Rinzel, 1998; Smith, Owens, & Forsythe, 2000; Palmer, Shackleton, & McAlpine, 2002).

The initial processing of interaural timing cues occurs in the medial superior olive (MSO) in which neurons receive excitatory input from the large, spherical, bushy cells of both (right and left) antro ventral cochlear nucleus (AVCN), which preserve, and even enhance, the timing accuracy seen in the auditory nerve, providing exquisitely timed inputs (Warr, 1966, 1969; Palmer et al., 2002; Joris, Carney, Smith, & Yin, 1994). These types of cells are frequently called excitatory-excitatory (EE) cells (e.g., Guinan, Guinan, & Norris, 1972; Joris et al., 1994).

Another type of CD cell is found in the lateral superior olive (LSO), where neurons receive inhibitory inputs from neurons in the ipsilateral medial nucleus of the trapezoid body (MNTB), which in turn receive excitatory input from the globular bushy cells of the contralateral cochlear nucleus (Glendenning, Hutson, Nudo, & Masterton, 1985; Cant, 1991; Warr, 1972; Boudreau & Tsuchitani, 1968). The pathway from AVCN to MNTB is characterized by synapses producing secure, short-latency responses and therefore near-coincident arrival at the LSO of the ipsilateral excitation and the contralateral inhibition. Those neurons are sensitive to the balance of intensity at the ears because the excitation due to ipsilateral sounds is reduced by increasing levels of contralateral sounds (Boudreau & Tsuchitani, 1970;

Guinan et al., 1972; Caird & Klinke, 1983; Caspary & Finlayson, 1991). Those cells are frequently referred as excitatory-inhibitory (EI) cells (e.g., Guinan et al., 1972; Tollin & Yin, 2002).

Existing computational methods for neural cells analysis can explain the functionalities of a general CD cell. Several computational methods are biological constraints that can be used to investigate the type of information emerging from within the brain's neural activity in neural cells (Herz, Gollisch, Machens, & Jaeger, 2006). For example, in integrate-and-fire models (reviewed by Burkitt, 2006a, 2006b), the cell neural membrane potential is obtained by applying a decision rule. Whenever the membrane potential crosses a given threshold, the cell generates spikes. A complete neural net might include a thousand or more cells, and Monte Carlo simulation can yield a description of the neural system (e.g., Amemori & Ishii, 2001).

Another way to characterize the neural system behavior as a function of input stimuli is by analyzing the stochastic properties of each level in the brain and of each type of neural cell. The output of such a system can be used to predict known behavioral properties. Such a computational method was used for the auditory nerve where just noticeable differences (JND) of a tone's frequency, level, and interaural cues were predicted (Siebert, 1968, 1970; Colburn, 1973; Stern & Colburn, 1978; Heinz, 2000; Heinz, Colburn, & Carney, 2001; Cohen, Furst, & Krips, 2004).

Hohn and Burkitt (2001) and Lowen and Teich (1996) derived an analytical description of neural processing assuming a stationary input. As most natural signals are not stationary, elucidating analytically the stochastic properties of each level in the neural pathway can lead to a more comprehensive analysis of the brain function.

In this letter, we analytically compute the probability density function of a set of spikes generated by a CD cell whose inputs are sets of spikes that behave as NHPP. Those derivations can be further used to predict binaural behavioral properties, for example, binaural perception (Krips & Furst, 2009; Krips, 2008).

2 Characterization of CD Cell Inputs

A CD cell receives independent neural inputs and generates neural output. Each neural input is presented by a set of spikes that occur at instances $\{t_i, i \geq 1\}$. This series of action potentials behaves as a random point process with instantaneous rate $\lambda(t)$ and refractory period τ_r. The probability of obtaining $n_s = n$ spikes in the interval $[0, T_e)$ is equal to

$$P(n_s = n) = \frac{(\Lambda(T_e))^n}{n!} e^{-\Lambda(T_e)}, \tag{2.1}$$

where n_s is the number of generated spikes and $\Lambda(T_e)$ is the expected number of spikes in the interval $[0, T_e)$ and is given by

$$\Lambda(T_e) = \int_0^{T_e} \lambda(t)\, dt. \tag{2.2}$$

The normalized instantaneous rate $\lambda^*(t)$ is equal to the probability that a spike occurs at a given interval $t \in [0, T_e)$ given there are n spikes in the interval $[0, T_e)$ (Snyder & Miller, 1991):

$$\lambda^*(t) = P(t_k = t \mid n_s = n) = \frac{\lambda(t)}{\Lambda(T_e)}. \tag{2.3}$$

An equivalent definition of an NHPP to equation 2.1 is by the probability density function of the interval length between successive spikes (Lewis & Shedler, 1978; Brown, 1984; Snyder & Miller, 1991). In an NHPP, the intervals are independent and exhibit an exponential distribution,

$$\left.\begin{aligned} p(t_{k+1} - t_k > T \mid t_k = x) &= \exp\left(-\int_x^{x+T} \lambda(t)\, dt\right) \\ P(t_{k+1} - t_k > T \mid t_k = x, Y) &= P(t_{k+1} - t_k > T \mid t_k = x) \end{aligned}\right\} \tag{2.4}$$

where Y is an arbitrary event that occurred in the past, before the current interspike interval.

In the rest of the letter, we show that CD output exhibits NHPP behavior by equation 2.4. For simplicity and without loss of generality, in the rest of the letter, we choose $t_k = 0$.

3 An Excitatory-Inhibitory Cell Model

3.1 Simple Model with Two Inputs. A simple excitatory-inhibitory (EI) cell has two asymmetric inputs: excitatory (E) and inhibitory (I). Their instantaneous rates are denoted by λ_E and λ_I for the excitatory and inhibitory inputs, respectively. Similarly, the refractory periods are denoted by $\tau_r^{(E)}$ and $\tau_r^{(I)}$, respectively. An EI cell spikes whenever the excitatory input spikes and in the preceding Δ seconds ($\Delta > 0$), the inhibitory input does not spike. Therefore, if in the period T there are n_E and n_I instances in the excitatory and inhibitory inputs, respectively, the EI cell will generate a spike at $t_j^{(E)}$ $(1 \le j \le n_E)$ if none of the inhibitory inputs $t_i^{(I)}$ $(1 \le i \le n_I)$ satisfies the condition $0 < t_j^{(E)} - t_i^{(I)} < \Delta$. To avoid the case that more than one excitatory spike can occur during Δ, we add to the definition of *EI* the constraint $\Delta < \tau_r^{(E)}$.

Formally, the EI output includes sets of spikes that occur at instances $\{t_k^{(EI)}, k \geq 1\}$ where

$$t_k^{(EI)} = t_j^{(E)} \; if \; \exists j \;\; \forall i \;\; \{t_j^{(E)} - t_i^{(I)} > \Delta\} \bigcup \{t_j^{(E)} < t_i^{(I)}\}, \tag{3.1}$$

where $1 \leq i \leq n_I$ and $1 \leq j \leq n_E$.

Let us define as $\overline{EI}$ the event in which the interval between successive spikes in the *EI* cell output exceeds T seconds. Equation 3.1 implies that $\overline{EI}$ is the event in which no spike was generated by *EI* in T seconds. This is denoted by

$$\overline{EI} = \Big\{\{n_E = 0\} \bigcup \{0 < n_E \leq n_I, \; \forall t_p^{(E)} \; 1 \leq p \leq n_E \; \exists t_q^{(I)} \; 1 \leq q \leq n_I, \\ 0 < t_p^{(E)} - t_q^{(I)} < \Delta\}\Big\}. \tag{3.2}$$

According to the definition of an NHPP in equation 2.4, we will show in the following lemma that $p(\overline{EI})$ represents an NHPP, that is, its interspike intervals have an exponential distribution and they are statistically independent.

Lemma 1. *If $\Delta < \tau_r^{(E)}$, then $p(\overline{EI}) = \exp(-\Lambda_{EI}(T))$ when $\Lambda_{EI}(T) = \int_0^T \lambda_E(t)(1 - \int_{t-\Delta}^{t} \lambda_I(t')\,dt')\,dt$ for $\overline{EI}$, which is defined in equation 3.2. For any arbitrary event Y that occurred in the past, $P(\overline{EI} \mid Y) = P(\overline{EI})$.*

Proof. Since the definition of *EI* includes the constraint $\Delta < \tau_r^{(E)}$, in an interval whose length is less than or equal to Δ, only one excitatory spike can occur. Let us further assume that there are maximum M inhibitory and N excitatory spikes in the interval $[0, T)$. The definition of $\overline{EI}$ in equation 3.2 yields the probability of $\overline{EI}$, which is obtained by

$$P(\overline{EI}) = P(n_E = 0) + \sum_{n=1}^{\tilde{N}} P(n_E = n) \sum_{m=n}^{M} P(n_I = m) P\big(\forall t_p^{(E)} \exists t_q^{(I)}, \\ 0 < t_p^{(E)} - t_q^{(I)} < \Delta \mid n_E = n, n_I = m\big), \tag{3.3a}$$

where, $\tilde{N} = \min(N, M)$.

$P(\overline{EI} \mid Y)$ is given by

$$P(\overline{EI} \mid Y) = P(n_E = 0 \mid Y) \\ + \sum_{n=1}^{\tilde{N}} P(n_E = n \mid Y) \sum_{m=n}^{M} P(n_I = m \mid Y) P\big(\forall t_p^{(E)} \exists t_q^{(I)}, \\ 0 < t_p^{(E)} - t_q^{(I)} < \Delta \mid n_E = n, n_I = m, Y\big). \tag{3.3b}$$

Since all the probabilities in equation 3.3b are NHPP, the following conditions are satisfied:

$$\left.\begin{aligned} &P(n_E = 0 \mid Y) = P(n_E = 0),\\ &P(n_E = n \mid Y) = P(n_E = n),\\ &P(n_I = m \mid Y) = P(n_I = m),\\ &P\left(\forall t_p^{(E)}\, \exists t_q^{(I)},\ 0 < t_p^{(E)} - t_q^{(I)} < \Delta \mid n_E = n, n_I = m, Y\right) =\\ &P\left(\forall t_p^{(E)}\, \exists t_q^{(I)},\ 0 < t_p^{(E)} - t_q^{(I)} < \Delta \mid n_E = n, n_I = m\right) \end{aligned}\right\}.$$

The implication is that equations 3.3a and 3.3b are identical and, particularly, $P(\overline{EI} \mid Y) = P(\overline{EI})$.

The probability of the event $\{0 < t_p^{(E)} - t_q^{(I)} < \Delta \mid n_E = n, n_I = m\}$ that is included in equation 3.2 is obtained by

$$\begin{aligned} &P\left(0 < t_p^{(E)} - t_q^{(I)} < \Delta \mid n_E = n, n_I = m\right)\\ &\quad = \int_0^T P\left(t_p^{(E)} = t \mid n_E = n\right) P\left(t - \Delta < t_q^{(I)} < t \mid n_I = m\right) dt. \end{aligned} \tag{3.4}$$

Substituting equation 2.3 in equation 3.4 yields

$$\begin{aligned} &P\left(0 < t_p^{(E)} - t_q^{(I)} < \Delta \mid n_E\right.\\ &\left.\quad = n, n_I = m\right) = \int_0^T \lambda_E^*(t) \int_{t-\Delta}^t \lambda_I^*(t')\, dt' dt = \frac{\Lambda_o}{\Lambda_E \Lambda_I}, \end{aligned} \tag{3.5}$$

where

$$\Lambda_0 = \int_0^T \lambda_E(t) \int_{t-\Delta}^t \lambda_I(t')\, dt' dt. \tag{3.6}$$

Λ_E and Λ_I are equal to the expected number of spikes in an interval of length T of the excitatory and inhibitory inputs, respectively, similar to the definition in equation 2.2.

Since the probability that was derived in equation 3.5 is independent of q and p, the probability of given n inhibitory spikes exactly inhibiting n excitatory spikes is equal to $(\frac{\Lambda_0}{\Lambda_E \Lambda_I})^n$. In case there are more inhibitory spikes than excitatory spikes ($m > n$), a total of $(m)_n = m!/(m-n)!$ different choices will satisfy equation 3.3, that is,

$$P\left(\forall t_i^{(E)} \exists t_j^{(I)}, 0 < t_j^{(E)} - t_i^{(I)} < \Delta \mid n_E = n, n_I = m\right) = \frac{m!}{(m-n)!} \left(\frac{\Lambda_0}{\Lambda_E \Lambda_I}\right)^n. \tag{3.7}$$

Substituting equations 3.7 and 2.1 in equation 3.3 yields

$$P(\overline{EI}) = e^{-\Lambda_E} + e^{-\Lambda_E} \sum_{n=1}^{\tilde{N}} \frac{(\Lambda_0)^n}{n!} \sum_{m=n}^{M} \frac{(\Lambda_I)^{m-n}}{(m-n)!} e^{-\Lambda_I}$$

$$= e^{-\Lambda_E - \Lambda_I} \sum_{n=0}^{\tilde{N}} \frac{(\Lambda_0)^n}{n!} \Gamma_n, \tag{3.8}$$

where $\Gamma_n = \sum_{m=0}^{M-n} \frac{(\Lambda_I)^m}{m!}$. It is thus clear that for $M \gg 1$, $\Gamma_0 \to e^{\Lambda_I}$. For $n > 1$, Γ_n includes n terms that are less than Γ_0, that is, $\Gamma_n = \Gamma_0 - \sum_{m=M-n+1}^{M} \frac{(\Lambda_I)^m}{m!}$. It is easy to show that $\sum_{m=M-n+1}^{M} \frac{(\Lambda_I)^m}{m!} \to 0$ if for every term in the sum $\frac{(\Lambda_I)^m}{m!} < \frac{(\Lambda_I)^{m-1}}{(m-1)!}$, which implies that if $n < M + 1 - \Lambda_I$ then $\Gamma_n \to e^{\Lambda_I}$. Thus, for M $\gg$ 1,

$$\sum_{n=0}^{\tilde{N}} \frac{(\Lambda_0)^n}{n!} \Gamma_n \to e^{\Lambda_0 + \Lambda_I}. \tag{3.9}$$

Substituting equation 3.9 in equation 3.8 yields

$$P(\overline{EI}) = e^{-\Lambda_E + \Lambda_0} = e^{-\Lambda_{EI}}, \tag{3.10}$$

where

$$\Lambda_{EI} = \Lambda_E - \Lambda_0 = \int_0^T \lambda_E(t) \left(1 - \int_{t-\Delta}^{t} \lambda_I(t')\, dt'\right) dt. \tag{3.11}$$

The instantaneous rate of a simple EI cell output is obtained by applying equation 2.2 in equation 3.11, which yields

$$\lambda_{EI}(t) = \lambda_E(t) \left(1 - \int_{t-\Delta}^{t} \lambda_I(t')\, dt'\right) \tag{3.12}$$

3.2 Multiple Inhibitory EI Cell. A multiple inhibitory EI cell has one excitatory input (E) whose instantaneous rate (IR) is λ_E and M independent inhibitory inputs $\{I_1, \ldots, I_M\}$ with instantaneous rates $\{\lambda_{I_1}, \ldots, \lambda_{I_M}\}$. The multiple inhibitory EI cell spikes whenever the excitatory input spikes, and in the preceding Δ seconds ($0 < \Delta < \tau_r^{(E)}$), none of the inhibitory inputs spikes. Therefore, the multiple inhibitory EI cell can be described as a string of M EI cells (see Figure 1). Each of the M EI cells receives a different inhibitory input. After the first simple EI cell in the string receives the original excitatory input (E), the second simple EI cell receives the output

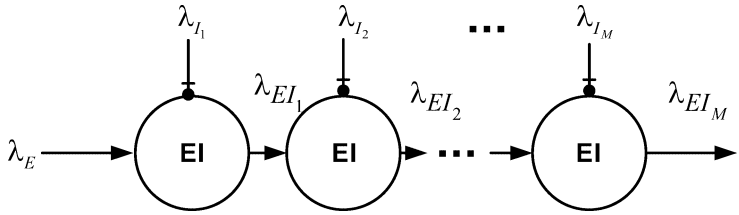

Figure 1: Multiple inhibitory EI cell implementation as a string of simple EI cells.

of the first simple EI cell as an excitatory input and so on. Since the output of a simple EI cell with independent inputs behaves as an NHPP, the output of the string of EI cells also behaves as an NHPP whose IR is given in equation 3.12.

The IR of the multiple inhibitory EI cell output is obtained by the IRs of each of the simple EI cells in the string as follows:

$$\left.\begin{aligned} \lambda_{EI_1} &= \lambda_E \left[1 - \int_{t-\Delta}^{t} \lambda_{I_1}(\zeta)\, d\zeta\right] \\ \lambda_{EI_2} &= \lambda_{EI_1} \left[1 - \int_{t-\Delta}^{t} \lambda_{I_2}(\zeta)\, d\zeta\right] \\ &\vdots \\ \lambda_{EI_M} &= \lambda_{EI_{M-1}} \left[1 - \int_{t-\Delta}^{t} \lambda_{I_M}(\zeta)\, d\zeta\right]. \end{aligned}\right\} \tag{3.13}$$

Substituting $\lambda_{EI_j}(t)$ for $1 \le j \le M-1$ in $\lambda_{EI_M}(t)$ according to equation 3.13 yields

$$\lambda_{EI_M} = \lambda_E(t) \prod_{i=1}^{M} \left[1 - \int_{t-\Delta}^{t} \lambda_{I_i}(\zeta)\, d\zeta\right]. \tag{3.14}$$

It is clear from equation 3.14 that since the inhibitory inputs are independent, their order does not affect the resultant IR. Note that for $M = 1$, equation 3.14 is equal to equation 3.12.

4 An Excitatory-Excitatory Cell Model

4.1 Simple EE Cell. A simple EE cell has two independent symmetrical inputs (E_1 and E_2). Each neural input is presented by a set of spikes that occur at instances $\{t_i^{(E_1)}, i \ge 1\}$ and $\{t_i^{(E_2)}, i \ge 1\}$. The EE cell generates an output spike whenever both inputs spike within a time interval of less than

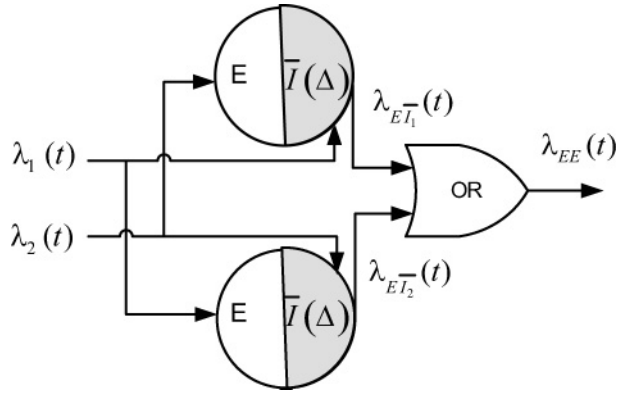

Figure 2: EE diagram as composed of $E\bar{I}$ cells. The $\bar{I}$ input is plotted in gray.

Δ seconds ($\Delta \geq 0$). EE generates a spike at $t_K^{(EE)}$ if there exist $t_i^{(E_1)}$ and $t_j^{(E_2)}$ that satisfy condition $|t_i^{(E_1)} - t_j^{(E_2)}| < \Delta$ and $t_k^{(EE)} = \max(t_i^{(E_1)}, t_j^{(E_2)})$.

In an NHPP, the probability of receiving an instance at a given time t is negligible, which implies that for any given i and j, $prob(t_i^{(E_1)} = t_j^{(E_2)}) \to 0$. Thus, without losing the generality, we can assume that $|t_i^{(E_1)} - t_j^{(E_2)}| > 0$. Therefore, a simple EE cell output includes a set of spikes $\{t_k^{EE},\ k > 1\}$ where

$$t_k^{(EE)} = \max\left\{t_i^{(E_1)}, t_j^{(E_2)}\right\} \quad if\ \exists i, j\ \ \left|t_i^{(E_1)} - t_j^{(E_2)}\right| < \Delta. \tag{4.1}$$

Note that $\{|t_i^{(E_1)} - t_j^{(E_2)}| < \Delta\} = \{0 < t_i^{(E_1)} - t_j^{(E_2)} < \Delta\} \cup \{0 < t_j^{(E_2)} - t_i^{(E_1)} < \Delta\}$. It is therefore possible to describe an EE cell as an OR combination of two cells that each can generate a spike that corresponds to the EE spike ($t_k^{(EE)}$). We call each of those cells $E\bar{I}$. They are sketched in Figure 2 as two-color circles. The white half receives the excitatory (E) input and the gray half receives the noninhibitory ($\bar{I}$) input. An output spike is generated if a noninhibitory ($\bar{I}$) input was obtained at most Δ seconds before an excitatory spike. We chose the term *noninhibitory* ($\bar{I}$) input and $E\bar{I}$ cell, correspondingly, since its definition complements the definition of *EI* cell (see equation 3.1). The difference between the two cells is that in the EI cell, the first spike (I) inhibits the second spike (E), while in the $E\bar{I}$ cell, the first spike ($\bar{I}$) enables the second spike (E).

The two inputs E and $\bar{I}$ are independent and are presented by a set of spikes: $\{t_i^{(E)}, i \geq 1\}$ and $\{t_i^{(\bar{I})}, i \geq 1\}$. The output of the $E\bar{I}$ cell generates spikes at $t_k^{(E\bar{I})}$, where

$$t_k^{(E\bar{I})} = t_j^{(E)}\ if\ \exists j, l\ 0 < t_j^{(E)} - t_l^{(\bar{I})} < \Delta. \tag{4.2}$$

Both of the $E\overline{I}$ cells, which together build the EE cell, receive the original inputs E_1 and E_2 that act as E or $\overline{I}$ inputs alternatively. The $E\overline{I}$ cells' outputs are denoted as $E\overline{I}_1$ and $E\overline{I}_2$, respectively. Thus, the possibility that $\exists j,l\ t_j^{(E)} = t_l^{(\overline{I})}$ may be excluded from the definition of an $E\overline{I}$ cell results in $\{t_i^{(E\overline{I}_1)}, i \geq 1\} \cap \{t_j^{(E\overline{I}_2)}, j \geq 1\} = \emptyset$. The EE output includes the following series of spikes: $\{t_i^{(E\overline{I}_1)}, i \geq 1\} \cup \{t_j^{(E\overline{I}_2)}, j \geq 1\}$, which have exactly the same incidences that were included in equation 4.1. In order to show that the EE cell output behaves as an NHPP, it is enough to prove that each $E\overline{I}$ cell output behaves as an NHPP.

Let us define an event $\overline{E\overline{I}}$ as one in which two successive spikes $(t_i^{(E\overline{I})}, t_{i+1}^{(E\overline{I})})$ of an $E\overline{I}$ cell output exceed T seconds. From equation 4.2, it implies that

$$\overline{E\overline{I}} = \left\{t_p^{(E)} - t_q^{(\overline{I})} > \Delta \quad or \quad t_p^{(E)} - t_q^{(\overline{I})} < 0; \quad \forall 0 \leq t_p^{(E)} < T, 0 \leq t_q^{(\overline{I})} < T\right\}. \tag{4.3}$$

As was indicated in equation 2.4, in order to prove that $E\overline{I}$ output behaves as an NHPP, we show in the following lemma that $p(\overline{E\overline{I}})$ behaves as a descending exponential:

Lemma 2. *For $\overline{E\overline{I}}$, which is defined in equation 4.3, and $\Delta \ll \tau_r^{(\overline{I})}$, then $p(\overline{E\overline{I}}) = \exp(-\Lambda_{E\overline{I}}(T))$, where $\Lambda_{E\overline{I}}(T) = \int_0^T \lambda_E(t) \int_{t-\Delta}^t \lambda_{\overline{I}}(t')\,dt'dt$ and $\tau_r^{(\overline{I})}$ is the refractory time of the $\overline{I}$ type input. For any arbitrary event Y that occurred in the past, $p(\overline{E\overline{I}} \mid Y) = p(\overline{E\overline{I}})$.*

Proof. Let us define the maximum possible number of input spikes to an $E\overline{I}$ cell in an interval $[0, T)$ as N_E and $N_{\overline{I}}$ for the E and $\overline{I}$ inputs, respectively. Note that for both inputs, the refractory time is positive, which yields a finite number of spikes in a finite interval. The actual number of spikes in the E and $\overline{I}$ inputs is denoted by n_E and $n_{\overline{I}}$, where $n_E \leq N_E < \infty$ and $n_{\overline{I}} \leq N_{\overline{I}} < \infty$. Based on the number of spikes entering the $E\overline{I}$ cell in the interval $[0, T)$, the event $\overline{E\overline{I}}$ can be defined as a combination of $(N_E + 1)X(N_{\overline{I}} + 1)$ independent events:

$$\overline{E\overline{I}} = \bigcup_{i=0}^{N_E} \bigcup_{j=0}^{N_{\overline{I}}} \{\overline{E\overline{I}}, n_E = i, n_{\overline{I}} = j\}, \tag{4.4}$$

and the probability of $\overline{E\bar{I}}$ can be expressed as

$$P(\overline{E\bar{I}}) = \sum_{i=0}^{N_E} P(n_E = i) \sum_{j=0}^{N_{\bar{I}}} P(n_{\bar{I}} = j) P(\overline{E\bar{I}} \mid n_E = i, n_{\bar{I}} = j). \tag{4.5a}$$

$P(\overline{E\bar{I}} \mid Y)$ is given by

$$P(\overline{E\bar{I}} \mid Y) = \sum_{i=0}^{N_E} P(n_E = i \mid Y) \sum_{j=0}^{N_{\bar{I}}} P(n_{\bar{I}} = j \mid Y) P(\overline{E\bar{I}} \mid n_E = i, n_{\bar{I}} = j, Y). \tag{4.5b}$$

From the definition of $\overline{E\bar{I}}$ in equation 4.4, it follows that for $n_E > 0$ and $n_{\bar{I}} > 0$,

$$\{\overline{E\bar{I}} \mid n_E = i, n_{\bar{I}} = j\} = \bigcap_{q=1}^{j} \overline{\bigcup_{p=1}^{i} \{0 < t_p^{(E)} - t_q^{(\bar{I})} < \Delta \mid n_E = i, n_{\bar{I}} = j\}}. \tag{4.6}$$

Since all the probabilities in equation 4.5b are NHPP and thus satisfy the following conditions,

$$\left.\begin{aligned} &P(n_E = i \mid Y) = P(n_E = i), \\ &P(n_{\bar{I}} = j \mid Y) = P(n_{\bar{I}} = j), \\ &P\big(0 < t_p^{(E)} - t_q^{(\bar{I})} < \Delta \mid n_E = i, n_{\bar{I}} = j, Y\big) \\ &\quad = P\big(0 < t_p^{(E)} - t_q^{(\bar{I})} < \Delta \mid n_E = i, n_{\bar{I}} = j\big) \end{aligned}\right\},$$

the implication is that equations 4.5a and 4.5b are identical, particularly $P(\overline{E\bar{I}} \mid Y) = P(\overline{E\bar{I}})$. The probability of the event $\{0 < t_p^{(E)} - t_q^{(\bar{I})} < \Delta \mid n_E = i, n_{\bar{I}} = j\}$ is obtained by

$$P\big(0 < t_p^{(E)} - t_q^{(\bar{I})} < \Delta \mid n_E = i, n_{\bar{I}} = j\big) = \int_0^T \lambda_E^*(t) \int_{t-\Delta}^{t} \lambda_{\bar{I}}^*(t') dt' dt = \frac{\Lambda_{E\bar{I}}}{\Lambda_E \Lambda_{\bar{I}}}, \tag{4.7}$$

where

$$\Lambda_{E\bar{I}} = \int_0^T \lambda_E(t) \int_{t-\Delta}^{t} \lambda_{\bar{I}}(t')\, dt' dt. \tag{4.8}$$

Since the resultant probability derived in equation 4.7 is independent of i and j, substituting its value in the probability for $\{\overline{E\bar{I}} \mid n_E = i, n_{\bar{I}} = j\}$ according to equation 4.6 yields

$$P(\overline{E\bar{I}} \mid n_E = i, n_{\bar{I}} = j) = \left(1 - i\frac{\Lambda_{E\bar{I}}}{\Lambda_E \Lambda_{\bar{I}}}\right)^j. \tag{4.9}$$

Substituting equations 4.9 and 2.1 in equation 4.5 yields

$$P(\overline{E\bar{I}}) = e^{-(\Lambda_E + \Lambda_{\bar{I}})} \sum_{i=0}^{N_E} \frac{\Lambda_E^i}{i!} \sum_{j=0}^{N_{\bar{I}}} \frac{\Lambda_{\bar{I}}^j}{j!} \left(1 - \frac{i\Lambda_{E\bar{I}}}{\Lambda_E \Lambda_{\bar{I}}}\right)^j. \tag{4.10}$$

Since $T \gg \max(\tau_r^{(E)}, \tau_r^{(\bar{I})})$, it implies that $N_E \gg 1$ and $N_{\bar{I}} \gg 1$; thus, $\lim_{N\to\infty} \sum_{i=0}^{N} \frac{x^i}{i!} = \exp(x)$ and equation 4.10 becomes

$$P(\overline{E\bar{I}}) = \exp(-\Lambda_E)\exp(\Lambda_{\bar{I}}\exp(-\Lambda_{E\bar{I}}/\Lambda_E)). \tag{4.11}$$

If $\Lambda_{E\bar{I}}/\Lambda_E \ll 1$, then $\exp\{-\Lambda_{E\bar{I}}/\Lambda_E\} \cong 1 - \Lambda_{E\bar{I}}/\Lambda_E$, which yields

$$P(\overline{E\bar{I}}) \approx \exp(-\Lambda_E)\exp(\Lambda_E(1 - \Lambda_{E\bar{I}}/\Lambda_E)) = \exp(-\Lambda_{E\bar{I}}). \tag{4.12}$$

Since $\int_{t-\Delta}^{t} \lambda_{\bar{I}}(t')\,dt' \le \Delta \cdot \max_{0\le t<T}\{\lambda_{\bar{I}}(t)\}$, it follows that

$$\frac{\Lambda_{E\bar{I}}}{\Lambda_E} = \frac{\int_0^T \lambda_E(t) \int_{t-\Delta}^{t} \lambda_{\bar{I}}(t')dt'dt}{\int_0^T \lambda_E(t)\,dt} \le \Delta \cdot \max_{0\le t<T} \lambda_{\bar{I}}(t). \tag{4.13}$$

On the other hand, the maximum instantaneous rate is limited by the refractory time,

$$\max_{0\le t<T} \lambda_{\bar{I}}(t) \le \frac{1}{\tau_r^{(\bar{I})}}, \tag{4.14}$$

which implies that

$$\frac{\Lambda_{E\bar{I}}}{\Lambda_E} \le \frac{\Delta}{\tau_r^{(\bar{I})}}. \tag{4.15}$$

It is therefore clear that if $\Delta \ll \tau_r^{(\bar{I})}$ then necessarily $\Lambda_{E\bar{I}}/\Lambda_E \ll 1$ and $p(\overline{E\bar{I}}) = \exp(-\Lambda_{E\bar{I}}(T))$.

An EE cell was defined as an OR product of two $E\bar{I}$ cells that both behave as NHPP if $\Delta \ll \tau_r^{(\bar{I})}$. Since both original inputs to the EE cell act as E and $\bar{I}$ inputs, alternatively, EE cell output behaves as an NHPP if $\Delta \ll$

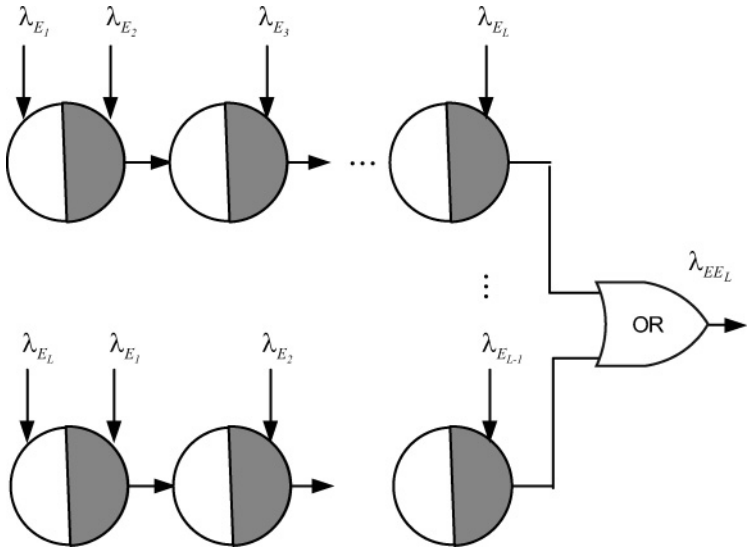

Figure 3: Implementation of an EE_L cell using strings of $E\overline{I}$ cells.

$\min\{\tau_r^{(E_1)}, \tau_r^{(E_2)}\}$, and the resultant instantaneous rate is $\lambda_{EE}(t) = \lambda_{E\overline{I}_1}(t) + \lambda_{E\overline{I}_2}(t)$. From equation 4.8, it follows that

$$\begin{aligned} \lambda_{E\overline{I}_1}(t) &= \lambda_2(t) \int_{t-\Delta}^{t} \lambda_1(t')\, dt' \\ \lambda_{E\overline{I}_2}(t) &= \lambda_1(t) \int_{t-\Delta}^{t} \lambda_2(t')\, dt', \end{aligned} \tag{4.16}$$

which implies that

$$\lambda_{EE}(t) = \lambda_1(t) \int_{t-\Delta}^{t} \lambda_2(t')\, dt' + \lambda_2(t) \int_{t-\Delta}^{t} \lambda_1(t')\, dt'. \tag{4.17}$$

4.2 Multiple Input EE Cell. A multiple input EE cell has N excitatory inputs $\{E_1, \ldots, E_N\}$ with instantaneous rates $\{\lambda_{E_1}, \ldots, \lambda_{E_N}\}$. It generates a spike whenever at least L of its inputs spikes during an interval Δ.

In order to prove that the output of the multiple input EE cell behaves as NHPP and to calculate its IR, we first assume that $N = L$ and denote it as EE_L. Such a cell generates a spike at the instances $\{t_k^{(EE_L)}, k \geq 1\}$, where

$$\begin{aligned} t_k^{(EE_L)} = \max\left\{t_{i_1}^{(E_1)}, \ldots, t_{i_L}^{(E_L)}\right\} \quad if\ \exists\, i_1, \ldots, i_L \quad \max\left\{t_{i_1}^{(E_1)}, \ldots, t_{i_L}^{(E_L)}\right\} \\ - \min\left\{t_{i_1}^{(E_1)}, \ldots, t_{i_L}^{(E_L)}\right\} < \Delta. \end{aligned} \tag{4.18}$$

The EE_L cell can be built as an OR combination of L strings of $E\overline{I}$ cells as depicted in Figure 3. Each string is built from $L - 1$ $E\overline{I}$ cells, with each cell

receiving a different noninhibitory input. The first $E\bar{I}$ cell in every string receives one of the E_i inputs as an excitatory input (E) and another input E_j as a noninhibitory input. The second $E\bar{I}$ cell in the string receives the output of the first $E\bar{I}$ cell as an excitatory input and E_k as a noninhibitory input when $k \neq i,\ j$. The other cells in the string are built in a similar way. The $L-1$ $E\bar{I}$ cells can be seen in Figure 3.

Let us denote the IR of the output of an $E\bar{I}$ cell in the string as $\lambda_{E\bar{I}_j}$ when the index j represents its position in the string. According to equation 4.16 and lemma 2, if $\Delta \ll \min\{\tau_r^{(E_1)}, \ldots, \tau_r^{(E_L)}\}$, then the output of each string behaves as NHPP and the IRs along the string are given by

$$\left.\begin{aligned} \lambda_{E\bar{I}_{L-1}} &= \lambda_{E\bar{I}_{L-2}} \left[\int_{t-\Delta}^{t} \lambda_{E_L}(t')\,dt'\right] \\ \lambda_{E\bar{I}_{L-2}} &= \lambda_{E\bar{I}_{L-3}} \left[\int_{t-\Delta}^{t} \lambda_{E_{L-1}}(t')\,dt'\right] \\ &\vdots \\ \lambda_{E\bar{I}_1} &= \lambda_{E_1} \left[\int_{t-\Delta}^{t} \lambda_{E_2}(t')\,dt'\right] \end{aligned}\right\}. \tag{4.19}$$

Substituting $\lambda_{E\bar{I}_j}(t)$ for $1 \leq j \leq L-2$ in $\lambda_{E\bar{I}_{L-1}}(t)$ according to equation 4.19 yields

$$\lambda_{E\bar{I}_{L-1}} = \lambda_{E_1} \prod_{l=2}^{L} \int_{t-\Delta}^{t} \lambda_{E_l}(t')\,dt'. \tag{4.20}$$

Since the inputs to the EE_L cell are independent, it is clear from equation 4.20 that the order of the $E\bar{I}$ cells in each string does not affect the resultant IR. Therefore, L different strings contribute the IR of an EE_L cell output and are combined by an OR gate, as shown in Figure 3. The resultant IR is obtained by

$$\lambda_{EE_L}(t) = \sum_{l=1}^{L} \lambda_{E_l}(t) \prod_{\substack{j=1 \\ j\neq l}}^{L} \int_{t-\Delta}^{t} \lambda_{E_j}(t')\,dt'. \tag{4.21}$$

A multiple input EE cell has N independent inputs and generates a spike when at least L of its inputs spike in an interval Δ. We now show that a multiple input EE cell can be built from EE_L cells.

Let us divide the group of inputs $\{E_1, \ldots, E_N\}$ into subgroups, each containing two sets of inputs. One set will contain l inputs to represent the inputs that generate a spike while a complementary set will include $N-l$ inputs to represent the inputs that do not spike. Let us denote the firing

inputs of the ith group as $\Psi_{l_i} = \{E_1^{(i)}, \ldots, E_l^{(i)}\}$ and the nonfiring group as $\Omega_{l_i} = \{E_{l+1}^{(i)}, \ldots, E_N^{(i)}\}$. For every choice of l, there are $\binom{N}{l}$ different possibilities when $L \leq l \leq N$. Therefore each of the possible subgroups includes all the EE cell's N inputs:

$$\{E_1, \ldots, E_N\} = \Psi_{l_i} \bigcup \Omega_{l_i} \quad 1 \leq i \leq \binom{N}{l}, \quad L \leq l \leq N. \tag{4.22}$$

For a given l_i, there are exactly l inputs that spike and $N - l$ inputs that do not spike during the interval Δ. This situation can be described as a string of two cells. The first cell, of type EE_l, includes l inputs, all of which should spike to generate an output spike. Its IR is derived by equation 4.21 and is denoted as $\lambda_{EE_L(\Psi_{l_i})}$ to indicate the type of cell and the group to which it has been applied. The second cell is a multiple input EI cell that receives the output of the EE_L as an excitatory input and $N - l$ inhibitory inputs. Its IR is derived by equation 3.14.

Let us denote an EE cell that spikes when exactly l of its inputs spike within Δ seconds as $EE_{=l}^N$. Its IR is obtained by combining all the possibilities of i, that is, $1 \leq i \leq \binom{N}{l}$, which reveals

$$\lambda_{EE_{=l}^N(\Psi)} = \sum_{i=1}^{\binom{N}{l}} \lambda_{EE_l(\Psi_{l_i})} \lambda_{I(\Omega_{l_i})}, \tag{4.23}$$

where

$$\lambda_{I(\Omega_{l_i})} = \prod_{E_j^{(i)} \in \Omega_{l_i}} \left(1 - \int_{t-\Delta}^{t} \lambda_{E_j^{(i)}}(t')\, dt'\right) = \prod_{j=l+1}^{N} \left(1 - \int_{t-\Delta}^{t} \lambda_{E_j^{(i)}}(t')\, dt'\right). \tag{4.24}$$

The multiple input EE cell that spikes when at least L of its inputs spike during an interval Δ is denoted as EE_L^N. Its IR is obtained by summing all the possibilities for $L \leq l \leq N$, which yields

$$\lambda_{EE_L^N(\Psi)} = \sum_{l=L}^{N} \lambda_{EE_{=l}^N(\Psi)}. \tag{4.25}$$

5 General CD Cell

A general CD cell is defined as one with N excitatory inputs $\Psi = \{E_1, \ldots, E_N\}$ and M inhibitory inputs, $\Omega = \{I_1, \ldots, I_M\}$. This type of cell generates a spike if, during an interval of length Δ, there are at least P more

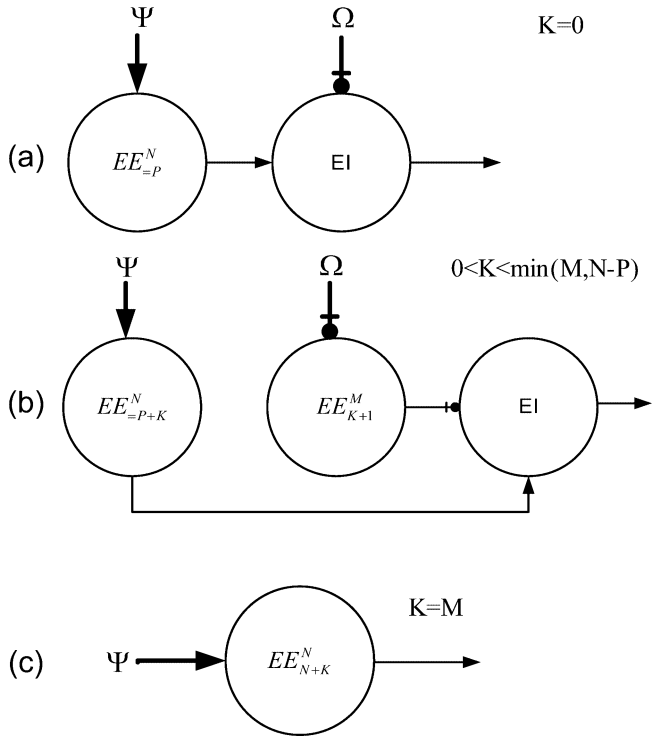

Figure 4: Breakdown of all functional alternatives for the general CD cell.

excitatory spikes than inhibitory spikes. A CD cell generates a spike in the following cases:

1. When exactly P excitatory inputs fire and none of the inhibitory inputs fires during a time interval Δ. Such a case can be described by a multiple input *EI* cell that receives the set Ω as inhibitory inputs and the output of $EE^N_{=P}$ cell as an excitatory input (see Figure 4a). The resultant IR is derived from equation 3.14, which yields $\lambda_{EE^N_{=P}(\Psi)} \cdot \lambda_{I(\Omega)}$.
2. When $P + K$ excitatory inputs fire, and at most K of the M inhibitory inputs fire during the time interval Δ when $0 < K < \min\{N - P, M\}$. An *EI* cell represents this case (see Figure 4b). Its excitatory input is the output of $EE^N_{=P+K}$ cell that is applied on the set Ψ, and its inhibitory input is the output of EE^M_{K+1} that is applied on the inhibitory set Ω. The resultant IR is obtained by equation 3.12, which yields

$$\lambda_{EE^N_{=P+K}(\Psi)} \left(1 - \int_{t-\Delta}^{t} \lambda_{EE^M_{K+1}(\Omega)}(t')\, dt'\right).$$

3. When $K > M$ and $P + K \leq N$, the CD cell will always generate a spike no matter how many inhibitory inputs are fired during the last Δ seconds. Such a case can be obtained only if $M < N - P$. The IR in this case will be the output of EE^N_{P+K} cell (see Figure 4c).

Thus, the IR of a general CD cell is obtained by

$$\lambda_{CD} = \sum_{k=0}^{\min(N-P,M)} \lambda_{CD_K}, \tag{5.1}$$

where

$$\lambda_{CD_K} = \begin{cases} \lambda_{EE^N_{=P}(\Psi)} \cdot \lambda_{I(\Omega)} & K = 0 \\ \lambda_{EE^N_{=P+K}(\Psi)} \left(1 - \int_{t-\Delta}^{t} \lambda_{EE^N_{K+1}(\Omega)}(t')\, dt'\right) & 1 \leq K \\ & \leq \min\{M-1, N-P\}. \\ \lambda_{EE^N_{P+K}(\Psi)} & K = M \end{cases} \tag{5.2}$$

6 Sample Results

6.1 Decrease of Spontaneous Rate. One of the properties of CD cells is a reduction in spontaneous rate (SR) when progressing across neural levels (Pfeiffer & Kiang, 1965; Tollin & Yin, 2002; Tollin, 2003; Ramachandran, Davis, & May, 1999).

In order to demonstrate the reduction in SR, we calculate the IR of an EE^N_L cell that receives N inputs and produces a spike when at least L of them spike during an interval Δ. The IR of all of its inputs is constant and equal to λ_{in}. The cell output IR is λ_{out}, which is derived by equation 4.25, which yields

$$\lambda_{out} = N! \sum_{l=L}^{N} \frac{(1 - \lambda_{in}\Delta)^{N-l}}{(N-l)!} \frac{\lambda_{in}^{l} \Delta^{l-1}}{(l-1)!}. \tag{6.1}$$

In Figure 5, λ_{out} is plotted as a function of N, for $L = 2$ and $\lambda_{in} =$ 20 spikes/sec for different values of Δ. In order to maintain the condition for the Poisson process, we chose $\Delta \cdot \lambda_{in} \leq 0.02$. As can be seen in Figure 5, λ_{out} increases with N and Δ. However, as a function of N, it increases moderately. If some of the N inputs are injured and thus inactive, the output of the CD cell will remain unchanged if $L \ll N$.

The increase in SR as a function of N can be moderated by a multilayered CD cell. The output of a low layer feeds the CD cells of the next layer.

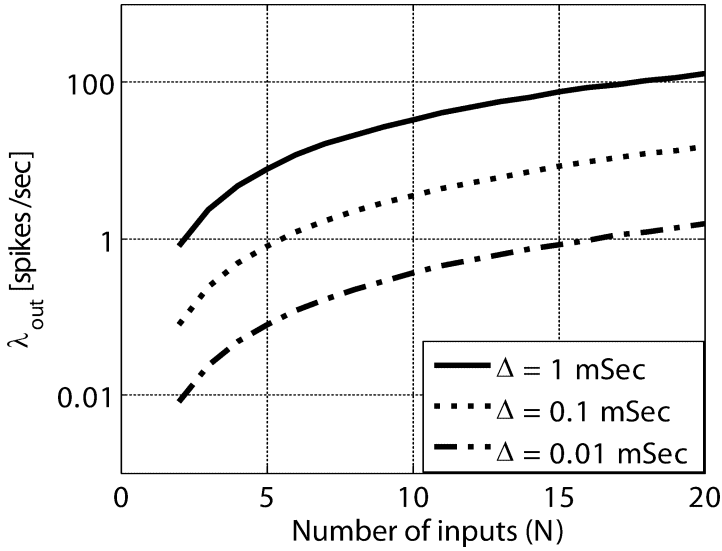

Figure 5: Spontaneous output rate as a function of number of inputs for several integration window sizes.

A network of EE_2^N type cells was designed. To maintain the independence of the inputs to each cell, the number of cells in every layer (g) was equal to N^{G-g}, when G is the maximum number of layers. λ_{out} of each layer was derived for $\lambda_{in} = 100$ spikes/sec, $\Delta = 0.5$ mSec, and $L = 2$ for different values of N and is plotted in Figure 6. It is clear from Figure 6 that both robustness and decrease in SR can be achieved. Increasing N causes an increase in SR but improves robustness. However, by increasing the number of layers, a significant decrease in SR can be gained.

6.2 SNR Improvement for Sinusoidal Inputs. Let us assume the following auditory nerve's IR for a sinusoidal input with a frequency ω:

$$\lambda_{in}(t) = A + \sin(wt). \tag{6.2}$$

Since any IR is nonnegative, we chose $A > 1$, to guarantee $\lambda_{in} > 0$. The initial SNR is thus

$$\mathrm{SNR_{in}} = 0.5/A^2. \tag{6.3}$$

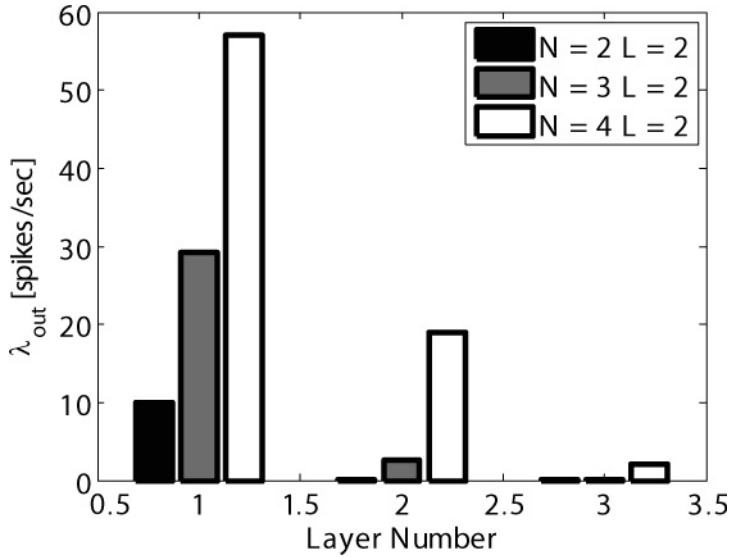

Figure 6: Output rate within a layered network as a function of layer number. The input rate equals 100 spikes/sec.

The IR of a simple EE cell was derived when both inputs have λ_{in}, as indicated in equation 6.2, and yielded

$$\lambda_{out}(t) = \frac{2}{w}\Big\{[A^2\Delta w + 0.5\sin(w\Delta)] + \sin(wt)[A\sin(\mathrm{w}\Delta) + A\Delta w] - \frac{\sin(\mathrm{w}\Delta)}{2}\cos(2wt)\Big\}. \tag{6.4}$$

For $\Delta \cdot \omega \ll 1$, equation 6.4 can be approximated as

$$\lambda_{out}(t) = \Delta\{[2A^2 + 1] + 4A\sin(wt)\}, \tag{6.5}$$

which yields

$$\mathrm{SNR_{out}} = 2\mathrm{A}^2/(A^2 + 0.5)^2. \tag{6.6}$$

The improvement in SNR as a function of the input SNR is shown in Figure 7a. The maximum SNR improvement of 6 dB was achieved for a relatively low-input SNR. The effect of Δ on the SNR improvement is shown in Figure 7b for different values of A. The SNR improvement vanishes with the increase of Δ, as can be expected from an efficient correlation processing.

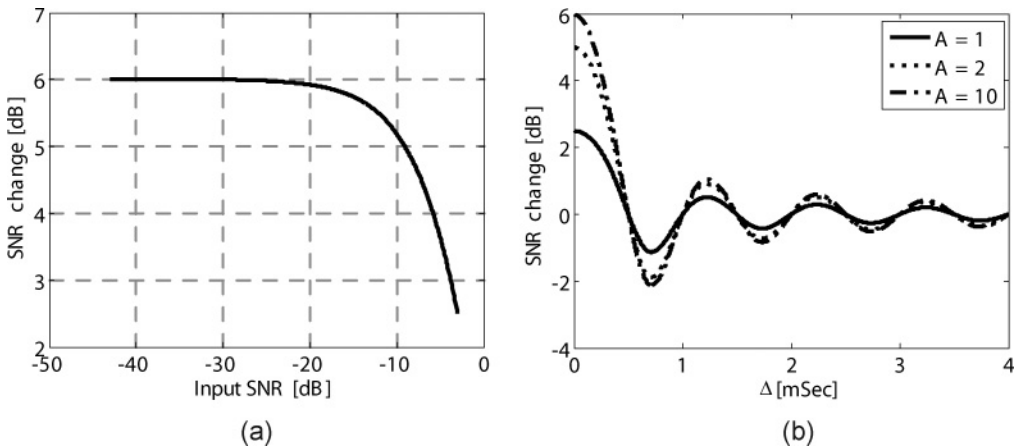

Figure 7: SNR improvement for an EE cell. (a) SNR change as a function of the input SNR. (b) SNR change as a function of integration duration for different input SNRs. Input frequency equals 1 KHz.

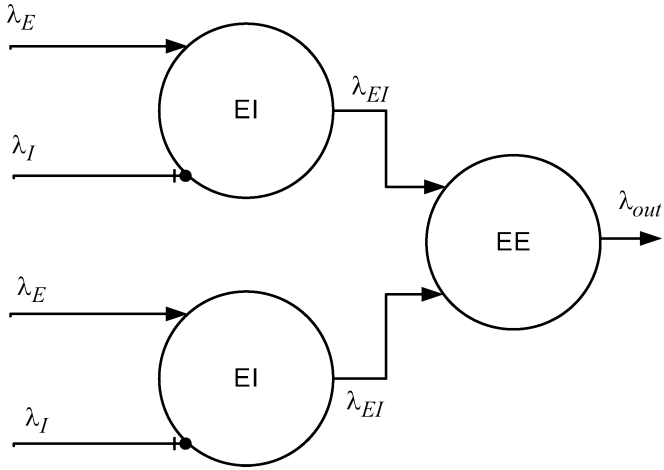

Figure 8: Sample EE EI combined network.

Another type of noise can be an undesired frequency (ω_n), $\omega_n \neq \omega_s$; for example, the IR can be

$$\lambda_1 = A + B\sin(\omega_s t) + C\sin(\omega_n t). \tag{6.7}$$

In order to reduce both components, the DC and ω_n, relative to the desired component, ω_s, a two-layer network as presented in Figure 8 can be applied. The first layer includes two EI cells, each receiving excitatory and inhibitory inputs. The IR of the excitatory input is obtained by

$$\lambda_E = \lambda_1, \tag{6.8}$$

where $\lambda_1$was defined in equation 6.7. The IR of the inhibitory input is given by

$$\lambda_I = D + E\sin(\omega_n t). \tag{6.9}$$

The normalized IRs, λ_E^* and λ_{EI}^* are plotted in Figure 9 in both time (panel a) and frequency (panel b) domains. The decrease of the ω_n component at the output of the first layer (λ_{EI}^*) is clearly shown. When a second layer of EE is applied, the ω_s component is significantly increased, as indicated in Figure 9b by λ_{out}^*. In general, EE cells increase common elements, whereas EI cells remove them.

6.3 LSO Cell's Response to Interaural Level Difference. Interaural level difference (ILD) is one of the most important cues for localizing high-frequency sounds (Irvine, 1992; Blauert, 1997). In mammals, ILD-sensitive neurons are found at almost every synaptic level from brainstem to cortex.

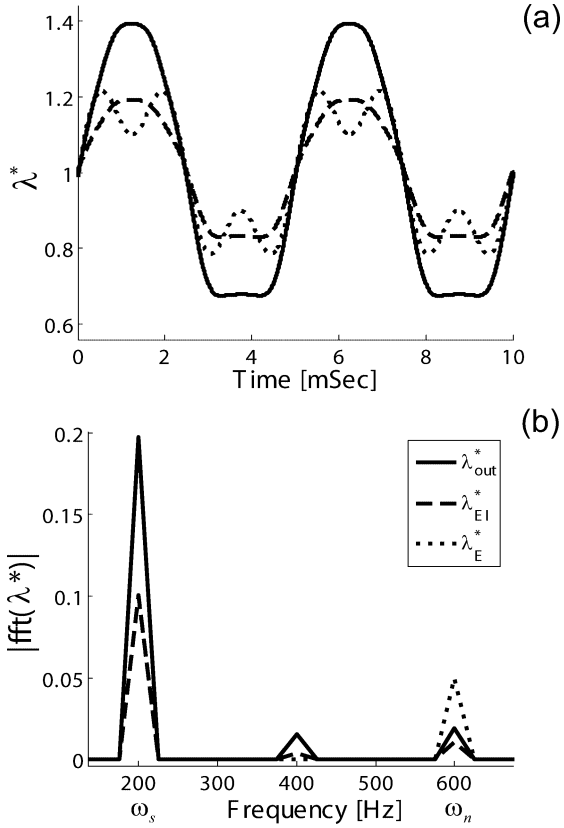

Figure 9: Network analysis across layers in time and frequency. The input is marked with a dotted line, the EI output with a dashed line, and the entire network as a solid line. (Upper panel) Time response. (Lower panel) Frequency response. DC component equals 1 for all layers. The parameters used are $A = 250$, $B = 50$, $C = 25$, $D = E = 400$ and an integration window for the EI cell 400 μSec and 40 μSec for the EE cell.

The first nucleus is the LSO (Boudreau & Tsuchitani, 1968; Caird & Klinke, 1983; Park, Klug, Holinstat, & Grothe, 2004). LSO cells receive excitatory inputs from the ipsilateral cochlear nucleus and inhibitory inputs from the contralateral medial nucleus of the trapezoid body, which is driven by the contralateral cochlear nucleus.

A typical LSO cell can be modeled as an EI cell with multiple excitatory and inhibitory inputs. Since LSO cells' characteristic frequency is high (above 3 kHz), the inputs' instantaneous rates are not synchronized to the stimulus, and therefore the mean rate is equal to the instantaneous rate. Substituting in equation 3.14, the mean input rates $\overline{\lambda}_{ipsi}$ and $\overline{\lambda}_{contra}$ for the

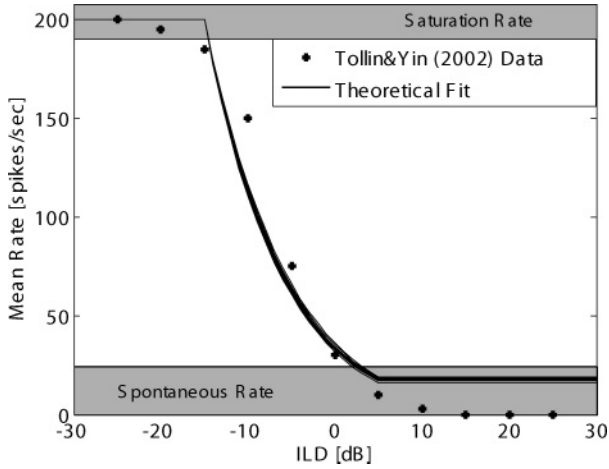

Figure 10: Mean discharge rate of an LSO cell as a function of ILD according to Tollin and Yin (2002) and according to an EI cell model.

ipsilateral and contralateral inputs, respectively, yield the mean rate of an EI cell with a single excitatory input and multiple inhibitory inputs:

$$\overline{\lambda}_{EI} = \overline{\lambda}_{ipsi}(1 - \Delta\overline{\lambda}_{contra})^{M}, \tag{6.10}$$

where M is the number of inhibitory inputs and Δ is the coincidence interval. $\overline{\lambda}_{EI}$ is plotted as a function of ILD in Figure 10. The derived mean rate was compared to experimental data (Tollin & Yin, 2002). The data points indicated in Figure 10 were obtained from Figure 1E in Tollin and Yin (2002). The data were collected from the LSO unit of an adult cat. The stimulus was 16 kHz tone, and the excitatory ear was held fixed at 30 dB SPL ($A_{ipsi} = 30$). The level to the contralateral ear (A_{contra}) was varied from 5 to 55 dB SPL. In order to predict the data, we used equation 6.10 with $\overline{\lambda}_{ipsi} = 200$ spikes/sec, and

$$\overline{\lambda}_{contra} = \begin{cases} 5 & A_{contra} \leq 15\ .5\ \text{dB SPL} \\ 10 \cdot (A_{contra} - 15) & 15\ .5 \leq A_{contra} \leq 35\ \text{dB SPL} \\ 200 & A_{contra} \geq 35\ \text{dB SPL} \end{cases}. \tag{6.11}$$

In order to fit equation 6.10 to the experimental data, we chose $\Delta < \tau_{r_E} = 5$ m sec. The data were fitted with $100 \leq \Delta \leq 1000$ μ sec. For every Δ, we calculated the correspondent number of inhibitory inputs (M_Δ) that yielded the minimum mean square error. All pairs (Δ, M_Δ) yielded a similar fit, as can be seen by the solid lines in Figure 10. The different lines merged almost

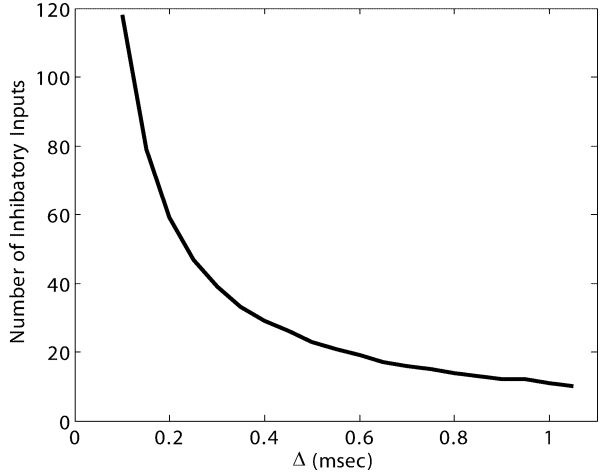

Figure 11: Optimal number of inhibitory inputs as a function of Δ (the coincidence interval) in an EI cell that best fits the experimental data.

to a single line. The dependence of M_Δ on Δ is shown in Figure 11, which reveals an increase of M_Δ with the decrease of Δ. Some studies indicate about 10 inhibitory inputs to LSO cells (Sanes, 1990; Shi & Horiuchi, 2004). Other studies indicate a larger number of inputs (Reed & Blum, 1990). A more extensive experimental study is required to resolve this issue.

7 Discussion

In this letter, we presented the stochastic properties of CD cells with both excitatory and inhibitory inputs, which we derived based on the initial assumption that all the inputs to the CD cell are independent and behave as NHPP. We proved analytically that both EE and EI outputs behave as NHPP. EI output requires that the coincidence interval (Δ) be shorter than the minimum refractory period of all its inputs, while Δ of EE is significantly smaller than the refractory period. This result means that the decision mechanism for generating a spike in a CD cell is terminated before any of its inputs generate a successive spike. In other words, the processing rate of a CD cell is faster than the incoming information rate, reflecting a robust, efficient, and reliable mechanism.

For the inhibitory inputs, the integration time must be smaller than the input information rate, while for the excitatory inputs, the integration time should be much smaller. We have shown that in general, EE cells increase common elements, whereas EI cells remove them. It seems that a shorter period of time is devoted to discovering and strengthening common elements, while a longer period is allowed for removing them.

It is quite clear that EE cells with their multiple inputs guarantee robustness, particularly in the case of lesions. Indeed, the system can perform almost normally when some of its parts are not functioning. While there will be some deterioration in the system's performance in the presence of serious defects, some functionality will remain.

Studies that measured Δ in different brain structures report values of the order of 10 microseconds and up to 100 microseconds in the lower parts of the auditory pathway (for excitatory inputs: Skottun, Shackleton, Arnott, & Palmer, 2001; Wagner, Brill, Kempter, & Carr, 2005; Agmon-Snir et al., 1998; Heinz, Colburn, & Carney, 2001; for inhibitory inputs: Brand, Behrend, Marquardt, McAlpine, & Grothe, 2002; Grothe, 2003; Siveke, Pecka, Seidl, Baudoux, & Grothe, 2006). The refractory period in those systems is on the order of 300 microseconds up to 1.3 milliseconds (Miller, Abbas, & Robinson, 2001; Bruce et al., 1999; Li & Young, 1993; Brown, 1994). At higher levels of the brain, the coincidence interval Δ is much higher and might reach milliseconds (Larkum, Zhu, & Sakmann, 1999). The refractory period can increase to the order of hundreds of milliseconds or even seconds (Larkum & Zhu, 2002; Sanchez-Vives & McCormick, 2000). Therefore, the requirement that Δ is significantly smaller than the refractory period of the coincidence inputs is valid for different brain structures.

The statistical properties of CD cell output were obtained by analytic calculation of the probability density function (pdf) of its spike train. The CD output was found to behave as an NHPP whose only parameter is the instantaneous rate (IR). The CD output's IR depends on only its inputs' IRs. The resulting closed form for the CD output IR implies that for any given feedforward neural system with CD cells, it is possible to calculate the pdf of the output of the entire system.

In this letter, we demonstrated this capability of the EE and EI cells with three simple examples: (1) a decrease in the spontaneous rate in the higher levels of the brain, (2) an improvement of the signal-to-noise ratio in EE cell output with sinusoidal (harmonic) inputs, and (3) a discharge rate change of EI cell as a function of interaural difference (ILD). Other properties of CD cells and their correspondence to binaural psychophysical performances were presented in detail in Krips and Furst (2009). In particular, it was shown that interaural time delay (ITD) is primarily estimated by EE cells and the ipsilateral auditory input exhibits a phase delay between 40 and 65 degrees as physiological data suggest (Yin & Chan, 1990; Palmer et al., 2002; McAlpine & Grothe, 2003; Hancock & Delgutte, 2004; Joris & Yin, 2007). ILD, on the other hand, is most likely estimated by EI cells, as was shown by physiological data (Tollin & Yin, 2002; Sanes, 1990; Reed & Blum 1990; Shi & Horiuchi, 2004; Glendenning et al., 1985; Cant, 1991; Warr, 1972; Boudreau & Tsuchitani, 1968).

CD cells are frequently found in different neural structures (Abeles, 1991). They can receive inputs from the same or different modalities. For example, CD cells have been identified in different levels of the auditory

system and recognized as an essential part of the localization mechanisms (Jeffress, 1948; Joris et al., 1998; Joris & Yin, 2007; Grothe, 2003; Kandler, 2004; McAlpine, 2005; Tollin & Yin, 2002).

The tools developed in this letter can serve in analyzing CD neural cell networks, which can lead to a better understanding of how the brain functions. We demonstrated the functionality of signal separation for EI and the integration of EE and EI into a single network. As well as presenting improved signal enhancement abilities, the network introduces the methodology of integrating both EE and EI components into a single cell since both result in NHPP spike trains.

The mathematical derivation in this letter was limited to a feedforward system whose inputs are independent and equally weighted. Most neural systems include both feedback (i.e., dependent inputs) and unequal weighted inputs (Kandel et al., 2000). It is possible to confront this discrepancy by assuming that for feedback paths that are long enough (e.g., periphery versus higher brain levels), the input that arrives from higher levels of the brain is independent of other inputs that arrive from lower parts in the brain. In order to account for the different weighted inputs to CD cells, it is possible to generalize from the derivation shown in this letter by referring different coincidence intervals to each of the different inputs. In this way, inputs with longer coincidence intervals can be considered stronger than inputs with shorter intervals. The condition for obtaining a NHPP in the CD output can then be expressed separately for each input (i.e., its coincidence interval should be smaller than its refractory period of the relevant input). However, the general result holds: the output behaves as an NHPP.

Acknowledgments

We thank Eli Merzbach and Yair Shaki for their inspiring discussions and comments.

References

Abeles, M. (1982). *Local cortical circuits: An electrophysiological study*. New York: Springer-Verlag.

Abeles, M. (1991). *Corticonics: Neural circuits of the cerebral cortex*. Cambridge: Cambridge University Press.

Agmon-Snir, H., Carr, C. E., & Rinzel, J. (1998). The role of dendrites in auditory coincidence detection. *Nature*, *393*, 268–272.

Amemori, K., & Ishii, S. (2001). Gaussian process approach to spiking neurons for inhomogeneous Poisson inputs. *Neural Computation*, *13*, 2763–2797.

Blauert, J. (1997). *Spatial hearing: The psychophysics of human sound localization* (rev. ed.). Cambridge, MA: MIT Press.

Boudreau, J. C., & Tsuchitani, C. (1968). Binaural interaction in the cat superior olive S segment. *Journal Neurophysiology*, *31*, 442–454.

Boudreau, J., & Tsuchitani, C. (1970). Cat superior olive S-segment cell discharge to tonal stimulation. *Contrib. Sens. Physiol.*, *4*, 143–213.

Brand, A., Behrend, O., Marquardt, T., McAlpine, D., & Grothe, B. (2002). Precise inhibition is essential for microsecond interaural time difference coding. *Nature*, *417*, 543–547.

Brown, M. C. (1994). Antidromic responses of single units from the spiral ganglion. *Journal of Neurophysiology*, *71*, 1835–1847.

Brown, T. C. (1984). "Poisson approximations and the definition of the Poisson process. *American Mathematical Monthly*, *91*, 116–123.

Bruce, I. C., Irlicht, L. S., White, M. W., O'Leary, S. J., Dynes, S., Javel, E., et al. (1999). A stochastic model of the electrically stimulated auditory nerve: Pulse-train response. *IEEE Trans. on Biomed. Eng.*, *46*, 630–637.

Burkitt, A. N. (2006a). A review of the integrate-and-fire neuron model: I. Homogeneous synaptic input. *Biological Cybernetics*, *95*, 1–19.

Burkitt, A. N. (2006b). A review of the integrate-and-fire neuron model: II. Inhomogeneous synaptic input and network properties. *Biological Cybernetics*, *95*, 1–19.

Caird, D. M., & Klinke, R. (1983). Processing of binaural stimuli by cat superior olivary complex neurons. *Experimental Brain Research*, *52*, 385–399.

Cant, N. B. (1991). Projections to the lateral and medial superior olivary nuclei from the spherical and globular bushy cells of the anteroventral cochlear nucleus. In R. A. Altschuler, R. P. Bobbin, B. M. Clopton, & D. W. Hoffman (Eds.), *Neurobiology of hearing: The central auditory system*. New York: Raven Press.

Carney, L. H. (1993). A model for the responses of low-frequency auditory-nerve fibers in cat. *J. Acoust. Soc. Am.*, *93*, 401–417.

Caspary, D. M., & Finlayson, P. G. (1991). Superior olivary complex: Functional neuropharmacology of the principal cell types. In R. P. Bobbin, B. M. Clopton, & D. W. Hoffman (Eds.), *Neurobiology of hearing: The central auditory system*. New York: Raven.

Cohen, O., Furst, M., & Krips, R. (2004). ITD and ILD estimation based on neural stochastic analysis. In *Proceedings of the 23rd IEEE Convention of Electrical and Electronics Engineers in Israel* (pp. 185–188). Piscataway, NJ: IEEE Press.

Colburn, S. H. (1973). Theory of binaural interaction based on auditory-nerve data. I. General strategy and preliminary results on interaural discrimination. *Journal of the Acoustical Society of America*, *54*(6), 1458–1470.

Gaumond, R. P., Kima, D. O., & Molnar, C. E. (1983). Response of cochlear nerve fibers to brief acoustic stimuli: Role of discharge-history effects. *J. Acoust Soc. Am.*, *74*, 1392–1398.

Glendenning, K. K., Hutson, K. A., Nudo, R. J., & Masterton, R. B. (1985). Acoustic chiasm II: Anatomical basis of binaurality in lateral superior olive of cat. *Journal of Comparative Neurology*, *232*, 261–285.

Goldberg, J. M., & Brown, P. B. (1969). Response of binaural neurons of dog superior olivary complex to dichotic tonal stimuli: Some physiological mechanisms of sound localization. *Journal of Neurophysiology*, *32*, 613–636.

Gray, P. R. (1967). Conditional probability analyses of the spike activity of single neurons. *Biophys J.*, *7*, 759–777.

Grothe, B. (2003). New roles for synaptic inhibition in sound localization. *Nat. Rev. Neurosci.*, *4*, 540–550.

Guinan, J. J., Guinan, S. S., & Norris, B. E. (1972). Single auditory units in the superior olivary complex. I. Responses to sounds and classifications based on physiological properties. *Int. J. Neurosci.*, *4*, 101–120.

Hancock. K. E., & Delgutte, B. (2004). A physiologically based model of interaural time difference discrimination. *Journal of Neuroscience*, *24*, 7110–7117.

Heinz, M. G. (2000). *Quantifying the effects of the cochlear amplifier on temporal and average-rate information in the auditory nerve*. Unpublished doctoral dissertation, MIT.

Heinz, M. G., Colburn, H. S., & Carney, L. H. (2001). Evaluating auditory performance limits: I. One-parameter discrimination using a computational model for the auditory nerve. *Neural Computation*, *13*, 2273–2316.

Herz, A. V. M., Gollisch, T., Machens, C. K., & Jaeger, D. (2006). Modeling single-neuron dynamics and computations: A balance of detail and abstraction. *Science*, *314*, 80–85.

Hohn N., & Burkitt A. N. (2001). Shot noise in the leaky integrate-and fire neuron. *Phys. Rev. E*, *63*, 031902.

Irvine, D. R. F. (1992). Physiology of the auditory brain stem. In A. N. Popper & R. R. Fay (Eds.), *The mammalian auditory pathway: Neurophysiology* (pp. 153–231). New York: Springer.

Jeffress, L. A. (1948). A place theory of sound localization. *J. Comp. Psychol.*, *44*, 35–39.

Johnson, D. H., & Swami, A. (1983). The transmission of signals by auditory-nerve fiber discharge patterns. *J. Acoust. Soc. Am.*, *74*, 493–501.

Joris, P. X., Carney, L. H., Smith, P. H., & Yin, T. C. T. (1994). Enhancement of neural synchronization in the anteroventral cochlear nucleus. I. Responses to tones at the characteristic frequency. *J. Neurophysiol.*, *71*, 1022–1036.

Joris, P. X., Smith, P. H., & Yin, T. C. T. (1998). Coincidence detection minireview in the auditory system: 50 years after Jeffress. *Neuron*, *21*, 1235–1238.

Joris, P. X., & Yin, T. C. T. (2007). A matter of time: Internal delays in binaural processing. *Trends Neurosci.*, *30*, 70–78.

Kandel, E. R., Schwartz, J. H., Jessell, M. J. (2000). *Principles of neural science* (4th ed.). New York: McGraw-Hill.

Kandler, K. (2004). Activity-dependent organization of inhibitory circuits: Lessons from the auditory system. *Curr. Opin. Neurobiol.*, *14*, 96–104.

Kiang, N. Y. S. (1965). *Discharge patterns of single fibers in the cat's auditory nerve*. Cambridge, MA: MIT Press.

Krips, R. (2008). Stochastic properties of coincidence-detector neural cells and their implications for binaural perception. Unpublished doctoral dissertation, Tel Aviv University.

Krips, R., & Furst, M. (2009). Stochastic properties of auditory brainstem coincidence detectors in binaural perception. *Journal of the Acoustical Society of America*, *125*, 1567–1583.

Larkum, M. E., & Zhu, J. J. (2002). Signaling of layer 1 and whisker-evoked Ca2+ and Na+ action potentials in distal and terminal dendrites of rat neocortical pyramidal neurons in vitro and in vivo. *Journal of Neuroscience*, *22*, 6991–7005.

Larkum, M. E., Zhu, J. J., & Sakmann, B. (1999). A new cellular mechanism for coupling inputs arriving at different cortical layers. *Nature*, *398*, 338–341.

Lewis, P. A. W., & Shedler, G. S. (1978). Simulation methods for Poisson processes in nonstationary systems. In *Proc. of the 10th Conference on Winter Simulation* (Vol. 1, pp. 155–163). Piscataway, NJ: IEEE Press.

Li, J., & Young, E. D. (1993). Discharge-rate dependence of refractory behavior of cat auditory-nerve fibers. *Hear. Res.*, *69*, 151–162.

Lowen, S. B., & Teich, M. C. (1996). The periodogram and Allan variance reveal fractal exponents greater than unity in auditory-nerve spike trains. *J. Acoust. Soc. of Am.*, *99*, 3585–3591.

McAlpine, D. (2005). Creating a sense of auditory space. *Journal of Physiology*, *566*, 21–28.

McAlpine, D., & Grothe, B. (2003). Sound localization and delay lines. Do mammals fit the model? *Trends in Neurosciences*, *26*, 347–350.

McAlpine, D., Jiang, D., Shackleton, T. M., & Palmer, A. R. (1998). Convergent input from brainstem coincidence detectors onto delay-sensitive neurons in the inferior colliculus. *J. Neurosci. 18*, 6026–6039.

Miller, C. A., Abbas, P. J., & Robinson, B. K. (2001). Response properties of the refractory auditory nerve fiber. *J. Assoc. Research in Otolaryngology*, *2*, 216–232.

Palmer, A. R., Shackleton, T. M., & McAlpine, D. (2002). Neural mechanisms of binaural hearing. *Acoust. Sci. and Tech.*, *23*, 61–68.

Park, T. J. (1998). IID sensitivity differs between two principal centers in the interaural intensity difference pathway: The LSO and the IC. *American Physiological Society*, *79*, 2416–2431.

Park, T. J., Klug, A., Holinstat, M., & Grothe, B. (2004). Interaural level difference processing in the lateral superior olive and the inferior colliculus. *Journal of Neurophysiology*, *92*, 289–301.

Pfeiffer, N., & Kiang, Y. S. (1965). Spike discharge patterns of spontaneous and continuously stimulated activity in the cochlear nucleus of anesthetized cats. *Biophysical Journal*, *5*, 301–316.

Ramachandran, R., Davis, K. A., & May, B. J. (1999). Single-unit responses in the inferior colliculus of decerebrate cats I. Classification based on frequency response maps. *Journal of Neurophysiology*, *82*, 152–163.

Reed, M. C., & Blum, J. J. (1990). A model for the computation and encoding of azimuthal information by the lateral superior olive. *Journal of the Acoustical Society of America*, *88*, 1442–1453.

Rieke, F., Warland, D., van Steveninck, R. D. R., & Bialek, W. (1997). *Spikes exploring the neural code*. Cambridge, MA: MIT Press.

Rodieck, R. W., Kiang, N. Y.-S., & Gerstein, G. L. (1962). Some quantitative methods for the study of spontaneous activity of single neurons. *Biophysical Journal*, *10*, 351–368

Rose, J. E., Brugge, J. L., Anderson, D. J., & Hind, J. E. (1967). Phase-locked response to low-frequency tones in single auditory nerve fibers of the squirrel monkey. *Journal of Neurophysiology*, *30*, 769–793.

Sanchez-Vives, M. V., & McCormick, D. A. (2000). Cellular and network mechanisms of rhythmic recurrent activity in neocortex. *Nature*, *3*, 1027–1034.

Sanes, D. H. (1990). An in vitro analysis of sound localization mechanisms in the gerbil lateral superior olive. *Journal of Neuroscience*, *2*, 3494–3506.

Shi, R. Z., & Horiuchi, T. K. (2004). A VLSI model of the bat lateral superior olive for azimuthal echolocation. In *Proceedings of the 2004 International Symposium on Circuits and Systems*. Piscataway, NJ: IEEE Press.

Siebert, W. M. (1968). Stimulus transformation in the peripheral auditory system. In P. A. Kolers & M. Eden (Eds.), *Recognizing patterns* (pp. 104–133). Cambridge, MA: MIT Press.

Siebert, W. M. (1970). Frequency discrimination in the auditory system: Place or periodicity mechanisms? *Proceedings IEEE*, *58*, 723–730.

Siveke, I., Pecka, M., Seidl, A. H., Baudoux, S., & Grothe, B. (2006). Binaural response properties of low-frequency neurons in the gerbil dorsal nucleus of the lateral lemniscus. *Journal of Neurophysiology*, *96*, 1425–1440.

Skottun, B. C., Shackleton, T. M., Arnott, R. H., & Palmer, A. R. (2001). The ability of inferior colliculus neurons to signal differences in interaural delay. *PNAS*, *98*, 14050–14054.

Smith, A. J., Owens, S., & Forsythe, I. D. (2000). Characterisation of inhibitory and excitatory postsynaptic currents of the rat medial superior olive. *J. Physiol.*, *529*, 681–698.

Snyder, D. L., & Miller, M. I. (1991). *Random point processes in time and space*. Berlin: Springer-Verlag.

Stern, R. M., Jr., & Colburn, H. S. (1978). Theory of binaural interaction based on auditory-nerve data. IV. A model for subjective lateral position. *J. Acoust. Soc. Am.*, *64*, 127–140.

Teich, M. C. (1989). Fractal character of the auditory neural spike train. *IEEE Trans. on Biomed. Eng.*, *36*, 150–160.

Teich, M. C., Heneghan, C., Lowen, S. B., Ozaki, T., & Kaplan, E. (1997). Fractal character of the neural spike train in the visual system of the cat. *Jour. Opt. Soc. Am. A*, *14*, 529–546.

Teich, M. C., & Khanna, S. M. (1985). Pulse-number distribution for the neural spike train in the cat's auditory nerve. *J. Acoust. Soc. Am.*, 1110–1128.

Tollin, D. J. (2003). The lateral superior olive: A functional role in sound source localization. *Neuroscientist*, *9*, 127–143.

Tollin, D. J., & Yin, T. C. T. (2002). The coding of spatial location by single units in the lateral superior olive of the cat. I. Spatial receptive fields in azimuth. *Journal of Neuroscience*, *22*, 1454–1467.

Wagner, H., Brill, S., Kempter, R., & Carr, C. E. (2005). Microsecond precision of phase delay in the auditory system of the barn owl. *J. Neurophysiol.*, *94*, 1655–1658.

Warr, W. B. (1966). Fiber degeneration following lesions in the anterior ventral cochlear nucleus of the cat. *Exp. Neurol.*, *14*, 453–474.

Warr, W. B. (1969). Fiber degeneration following lesions in the posteroventral cochlear nucleus of the cat. *Exp. Neurol.*, *23*, 140–155.

Warr, W. B. (1972). Fiber degeneration following lesions in the multipolar and globular cell areas in the ventral cochlear nucleus of the cat. *Brain Research*, *40*, 247–270.

Yin, T. C., & Chan, J. C. (1990). Interaural time sensitivity in medial superior olive of cat. *Journal of Neurophysiology*, *64*, 465–488.

Received July 5, 2007; accepted February 9, 2009.